Progress In Electromagnetics Research, Vol. 135, 563–581, 2013

WIDE SLOT LOOP ANTENNA WITH DISTANCE-ADJUSTABLE BACK-REFLECTOR FOR MULTIPLE NARROWBAND ANTENNAS REPLACEMENT

Peng Fei[1, *], Yihong Qi[2], and Yongchang Jiao[1]

[1]National Laboratory of Science and Technology on Antennas and Microwaves, Xi'an, Shaanxi, P. R. China

[2]DBJ Technologies, Zhuhai, Guangdong, P. R. China

Abstract—In this paper, a wide slot loop antenna with an adjustable back-reflector is introduced. Five working statuses are defined by simply adjusting the distances between the radiator and the reflector. Measured results show the total available operating band with better than 10 dB return loss ranges from 0.84 GHz to 3.04 GHz (113.4%). The radiation properties of the array are tested in an anechoic chamber. Stable unidirectional radiations with more than 8.3 dB gains are observed in the working band. Apart from that, the straightforward two-portion arrangement of the design provides cost-effective solution for mass production. All these features make the antenna an appropriate substitute for multiple narrowband antennas.

1. INTRODUCTION

As known to all, the antenna is one of the most crucial components in a communication system. Nowadays, with the rapid development of smart and multifunctional communication systems, antennas and antenna arrays with wide frequency coverage and reliable radiation properties are demanded [1–14]. Among various kinds of antennas, the slot loop antenna (SLA) has raised research interests in academic and industrial fields for its simple configuration and good radiation properties. Several such antennas have been demonstrated and discussed by researchers [15–18]. In these works, appreciated properties like low cross polarization level [15], omnidirectional patterns [16] and compact antenna size [17, 18] are achieved. However, the relative

Received 24 October 2012, Accepted 14 December 2012, Scheduled 2 January 2013

* Corresponding author: Peng Fei (pfei@mail.xidian.edu.cn).

bandwidths of these works are typically less than 10%, which limit their applications.

SLAs with wider impedance bandwidths are also developed in [19–21]. Cai and Ito in [19] presented the reflector-backed printed polygonal slot loop antenna with relative bandwidth of 24%. The antenna was designed based on the idea of combining a simple polygonal loop antenna and a rectangular slot antenna. Therefore, the antenna possesses the advantages of polygonal loop and rectangular slot antennas, such as high directivity and high tolerance in production. Mandal and Chen in [20] proposed an antenna combining a resonant strip loop with a slot loop for a dual-band and broadband operation. In [21], Low et al. proposed a wideband antenna for Ultra-Wideband (UWB) application. A microstrip-to-coplanar stripline (CPS) transition was also integrated to feed the radiation element. Lin and Wang in [22] proposed a broadband wide SLA (WSLA) employing delicate photonic band gap (PBG) structures to extend the impedance bandwidth of the antenna. In [23, 24], center-drive dual-element SLAs are introduced with bandwidths of 64% and 41%, respectively.

In the previous works, SLAs with wide impedance bandwidths are obtained. However, antennas with stable gains in wide frequency range are not as easy to be achieved. To maintain stable gain in wide band, an alternate solution is employing switching networks and multiple narrowband antennas with stable gains. Antenna engineers need to design several narrowband antennas with different dimensions, which is time consuming and cost-ineffective. The fact inspired us to develop a configurable SLA installation, which supplies reliable radiation and constant gain performance in different frequency bands therefore ease the design procedure. In this paper, a center-drive dual-element WSLA with wideband working potential is firstly introduced. The pony ear shaped slots and uplifted disc patches are employed in the design to introduce inductance and capacitance respectively. Detailed studies are given to some key parameters for better understanding the working mechanism of the loadings. Then a distance adjustable back-reflector is placed behind the radiator. By properly selecting the distance between the radiator and the reflector, five working statuses are defined. Reliable better than 8.3 dB gain performance is achieved in the band 0.84 GHz–3.04 GHz (113.4%) as the distance varies, which covers many commercial frequency bands, making the antenna a good candidate for multiple narrowband antennas replacement. The simple two-portion demountable arrangement of the design offers cost-effective solution for mass production, since it eases design and manufacture process. In addition, the solution also solves storage and inventory problems.

2. DESIGN OF THE CENTER-DRIVE WSLA

The geometry of the antenna is shown in Figure 1. The antenna is etched on commonly used FR4 substrate with relative permittivity $\varepsilon_r = 4.4$ and thickness $h = 1\,\text{mm}$. A microstrip to slotline Marchand balun [25, 26] is used to center-feed the configuration with $50\,\Omega$ input. Two symmetrical WSLA elements are back-to-back arranged. The inner perimeter of the WSLA element is chosen to be approximately comparable with the half wavelength of the center working frequency. Pony ear shaped slots (A) and uplifted disc patch (B) are employed to

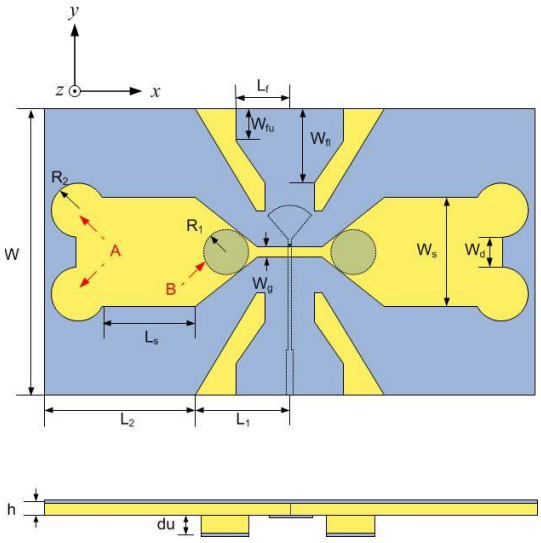

Figure 1. The geometry of the proposed antenna.

Table 1. Optimized dimension values.

Dimension	Value	Dimension	Value
W	93.4 mm	L_s	30.6 mm
W_s	35.3 mm	L_1	31.0 mm
W_d	10.0 mm	L_2	49.0 mm
W_{fu}	10.7 mm	R_1	8.6 mm
W_{fl}	24.0 mm	R_2	8.0 mm
W_g	3.7 mm	h	1.0 mm
L_f	8.1 mm	du	3.0 mm

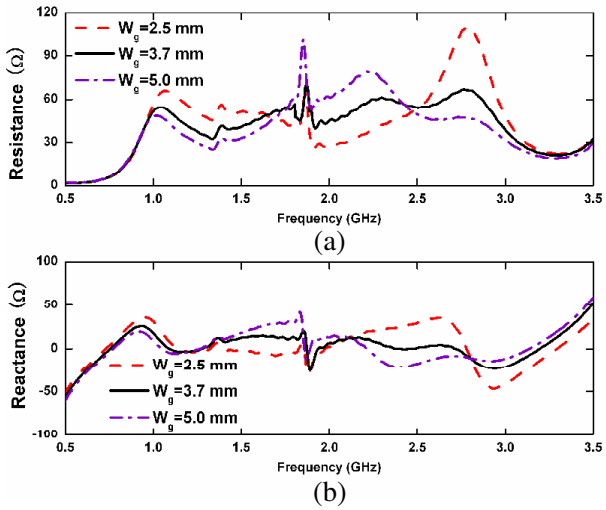

Figure 2. The (a) resistance and (b) reactance performances of the antenna with $W_g = 2.5\,\text{mm}$, $W_g = 3.7\,\text{mm}$ and $W_g = 5.0\,\text{mm}$.

extend the bandwidth of the antenna. Four cuts near the feeding region are applied to better smoothen the discontinuity from wide slotline to slot loop. The design parameters are defined in Figure 1. The optimized dimensions of these parameters are listed in Table 1. Some of the primary design parameters, for instance, slot width W_g, disc slot radius R_2 and the uplifted distance du, are studied in detail to examine their effects on the impedance matching performances of the antenna.

The proper selection of slot width W_g is crucial to guarantee the effective energy transition from microstrip to slotline. In fact, the slot with width W_g functions not only a part of the Marchand balun, but also plays an important role in the impedance matching of the antenna. Figure 2 shows the resistance and reactance performance of the antenna with $W_g = 2.5\,\text{mm}$, $3.7\,\text{mm}$ and $5.0\,\text{mm}$, respectively. When the slot width is too narrow ($W_g = 2.5\,\text{mm}$), the resistance of the antenna reaches up to $110\,\Omega$ in about 2.8 GHz, which mismatches the $50\,\Omega$ input. When the slot width increases to 5 mm, heavy protuberance is observed around 1.8 GHz. The figure also reveals that when $W_g = 3.7\,\text{mm}$, the in-band resistance curve is flatter and generally around $50\,\Omega$. The reactance variations plotted in Figure 2(b) indicates similar tendencies that best result is obtained when $W_g = 3.7\,\text{mm}$ among the three. Figure 3 shows the return loss performances of the antenna with the mentioned three W_g values. Clearly, when $W_g = 2.5\,\text{mm}$, the high

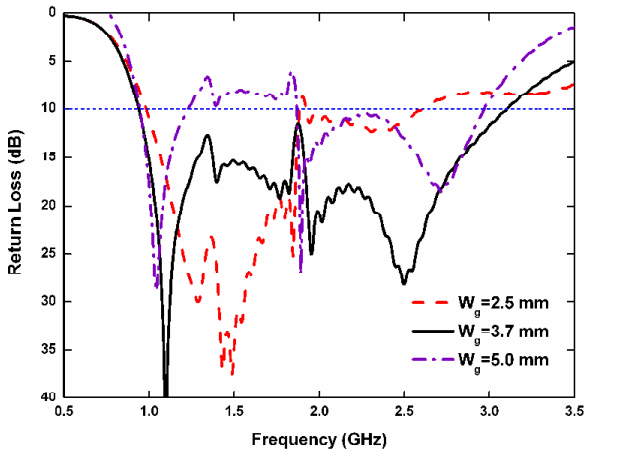

Figure 3. The return loss performances of the antenna with W_g = 2.5 mm, W_g = 3.7 mm and W_g = 5.0 mm.

end cut-off of the operating band is limited. On the other hand, when W_g = 5 mm, the reflection in the middle frequencies also restricted the antenna bandwidth. With respect to 10 dB return loss, widest operating band is achieved when W_g is chosen to be 3.7 mm.

The performances of the antenna with different sized pony ear shaped slots are also simulated. The size of the slots is defined by R_2 while R_2 = 0.0 mm stands for the situation that no pony ear shaped slot is etched on the antenna. It is worth to notice that the value of R_2 is also restricted by the antenna upper edge. The resistance and reactance performances are plotted in Figures 4(a) and (b), respectively. From Figure 4(a), as R_2 increases, the curves become flatter, indicating the wideband working potential. In Figure 4(b), as the size of the slot increases, more inductance is introduced and the curve is closer to zero. In Figure 5, it is also clear that as the size of the slots increases, the lower end of the band is extended to lower frequencies, which is appreciated for both antenna size miniaturization and relative bandwidth improvement.

The effects of the uplifted distance between the antenna slot loop and disc patch are evaluated as well. FR4 substrate is used to support the uplifted disc patch. In Figures 6 (a) and (b), the resistance and reactance performances of the antenna with different du values are respectively exhibited. The $du = inf$ case stands for the situation in which no disc patch is utilized while $du = 0$ stands for the situation that the disc patch are directly applied on the WLSA substrate. According

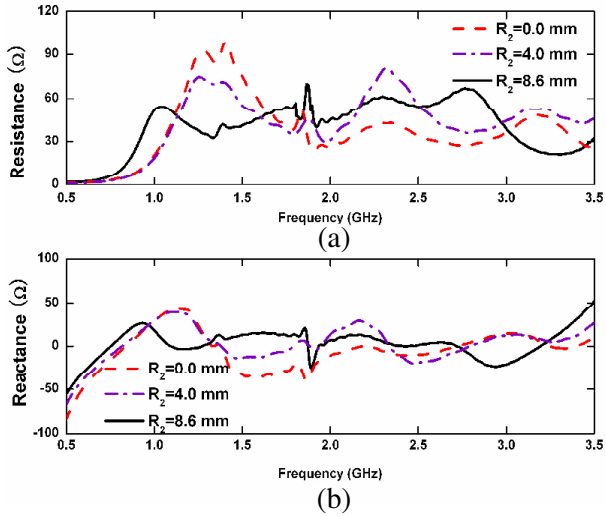

Figure 4. The (a) resistance and (b) reactance performances of the antenna with $R_2 = 0.0\,\text{mm}$, $R_2 = 4.0\,\text{mm}$ and $R_2 = 8.6\,\text{mm}$.

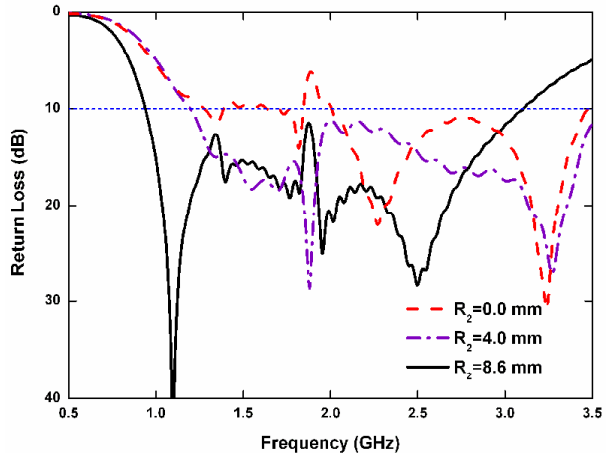

Figure 5. The return loss performances of the antenna with $R_2 = 0.0\,\text{mm}$, $R_2 = 4.0\,\text{mm}$ and $R_2 = 8.0\,\text{mm}$

to the figure, the $du = 3.0\,\text{mm}$ curve show more stable in band behavior compared with other two curves in Figure 6(a). In Figure 6(b), it can be seen the $du = 3.0\,\text{mm}$ curve is flatter and closer to zero. Figure 7

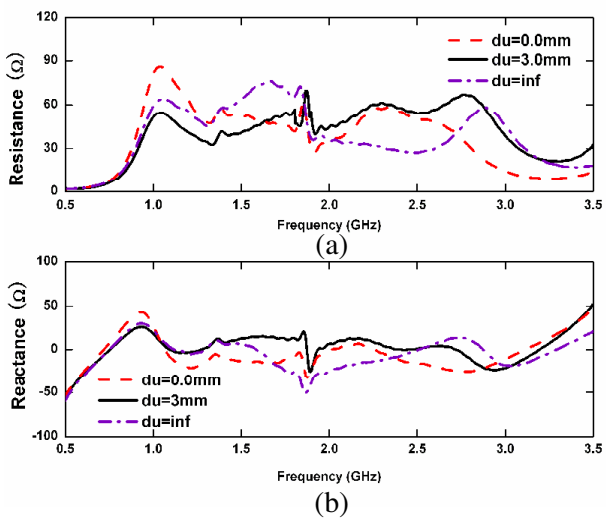

Figure 6. The (a) resistance and (b) reactance performances of the antenna with $du = 0.0\,\text{mm}$, $du = 3.0\,\text{mm}$ and $du = inf$.

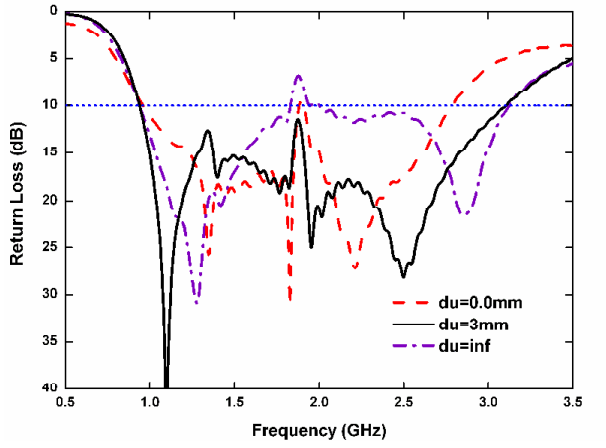

Figure 7. The return loss performances of the antenna with $du = 0.0\,\text{mm}$, $du = 3.0\,\text{mm}$ and $du = inf$.

shows the return loss performances of the antenna with different du values. When $du = 0$, with respect to 10 dB return loss, the high-end cut-off is limited to about 2.7 GHz. When $du = inf$, the high-end

cut-off reaches up to 3 GHz; however, protuberant behavior occurs in the middle frequency. When $du = 3.0$ mm, the operating band covers from 0.95 GHz to 3.1 GHz (106%), which is widest among the three. Adjusting the distance du is able to control the introduced capacitance to the antenna. Together with the pony ear shaped slots, which are inductive to the antenna, the resistance can be tuned to better increase the impedance bandwidth.

It is noticeable that there is a resonance at about 1.8 GHz for all analyzed cases. The resonance is not much affected by the variation of antenna dimensions analyzed above. The feeding microstrip to slotline transition is thus simulated. The average surface currents distributions at 1.7 GHz, 1.8 GHz and 1.9 GHz are obtained and plotted in Figure 8. From the figure, it is clear that compared with the situation at 1.7 GHz or 1.9 GHz, the currents are more concentrated around the microstrip stub at 1.8 GHz, which result in the resonance. Such resonance leads to a decline of antenna efficiency in corresponding frequency band.

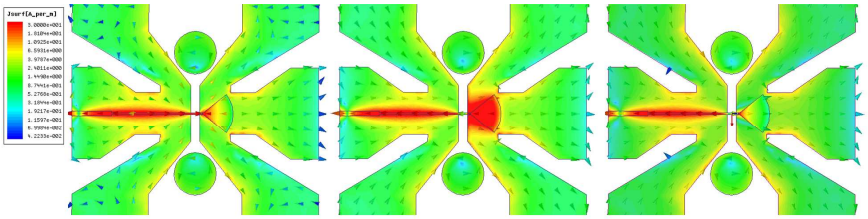

Figure 8. The surface currents distributions at (a) 1.7 GHz, (b) 1.8 GHz, and (c) 1.9 GHz.

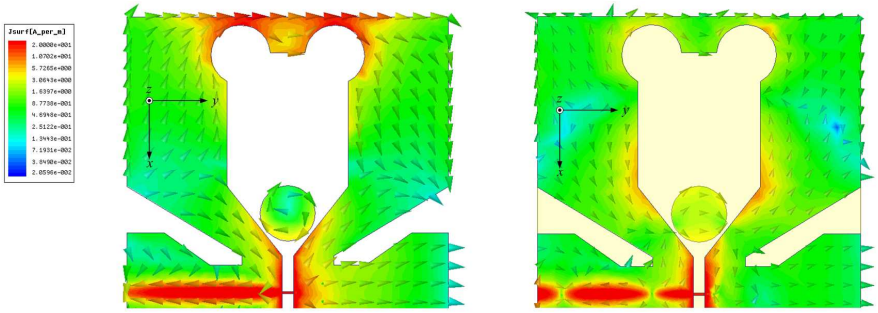

Figure 9. The surface current distributions of the proposed configuration at (a) 1 GHz and (b) 3 GHz.

However, further investment show that changing the dimension of the stub also cause impedance mismatch behaviors in the desired working band.

To further understand the working mechanism, the surface currents distributions on the antenna at 1 GHz and 3 GHz are simulated and plotted in Figures 9(a) and (b), respectively. Since the distributions of the currents are symmetrical at the mirrored elements, only part of the antenna configuration is shown in the figures. Generally, the surface currents along the transmission line and the cross junction region are intensive, indicating that the energy is efficiently coupled to the slotline. In Figure 9(a), it can be seen that at low frequency, the y-direction currents are intensively at the top edge of the slot loop. The x-direction currents along the two arms of the

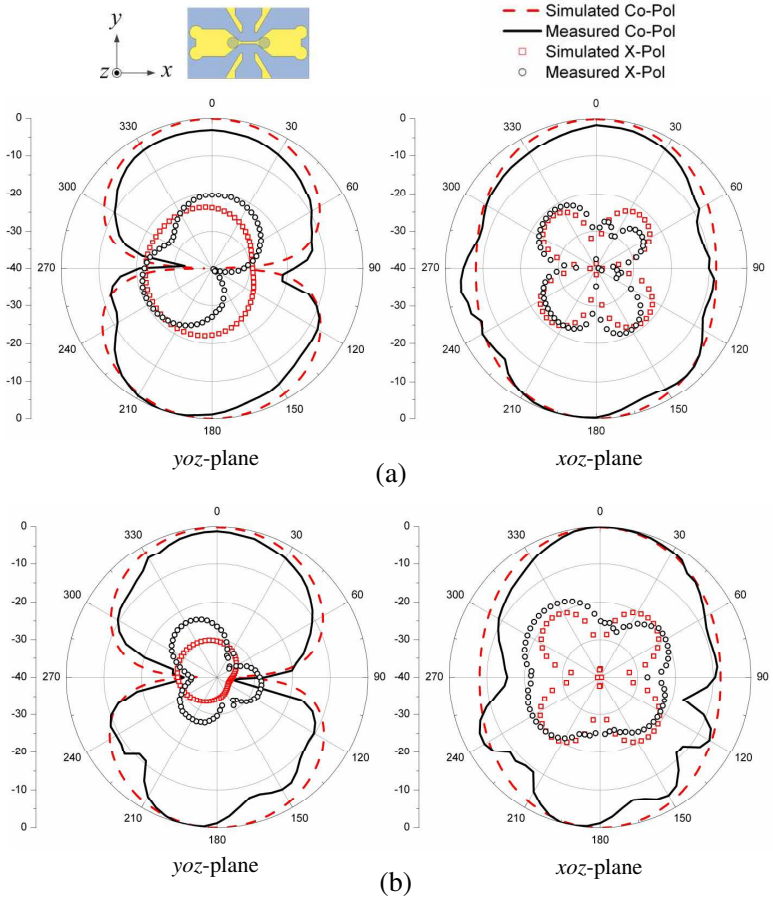

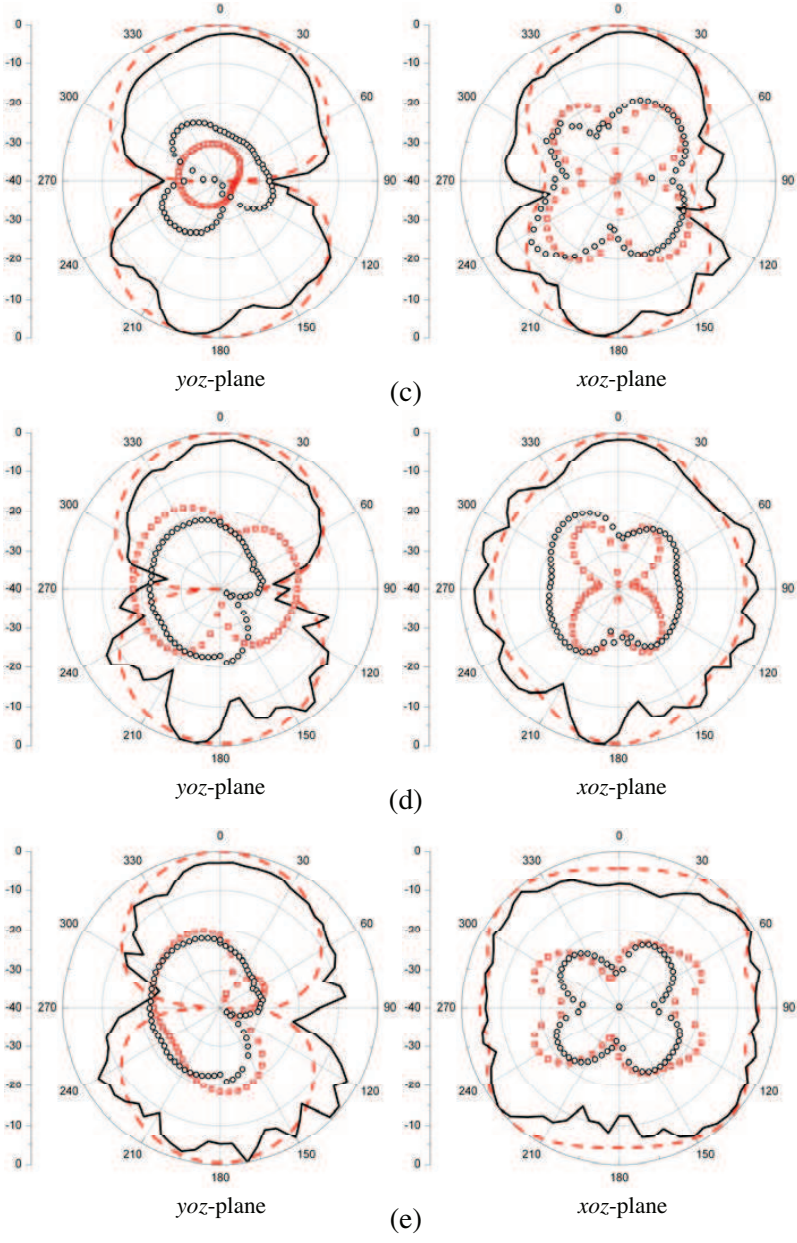

Figure 10. The simulated and measured normalized radiation patterns (in dB) of the WSLA at (a) 1.00 GHz, (b) 1.35 GHz, (c) 1.65 GHz, (d) 2.25 GHz and (e) 2.85 GHz.

polygonal slot are less intensive and out of phase, which cancel each other and suppress the unwanted cross polarization radiation. At higher frequency, as shown in Figure 9(b), apart from the top edge of the antenna, the both side edges of the tapered polygonal slot also become the main radiation portion. For the currents along the two sides of the slot, their y-direction components are in phase and reinforce each other; while the x-direction components are in opposite directions, which cancel each other.

A prototype of the WSLA is fabricated. The simulated and measured normalized radiation patterns of the antenna at different frequencies are shown in Figure 10. From the figure, it can be seen that the radiation patterns are bidirectional to $\pm z$-directions in most of its working band. The measured results agree well with the simulated ones in front beam ($+z$-direction). The measured ripples in the back beam ($-z$-direction) are mainly due to the test environment error. In yoz-plane, 8-shaped patterns are observed. The xoz-plane patterns, on the other hand, vary as frequency changes. In Figure 10(e), the maximum radiation direction in xoz-plane splits to $\pm 45^\circ$ directions. This is because as frequency increases, the electrical distance between the two WSLA elements is long enough that grating lobes emerge. Cross Polarization are also measured and shown in Figure 10. The Cross Polarization levels in maximum radiation directions are less than -20 dB in all the tested frequencies.

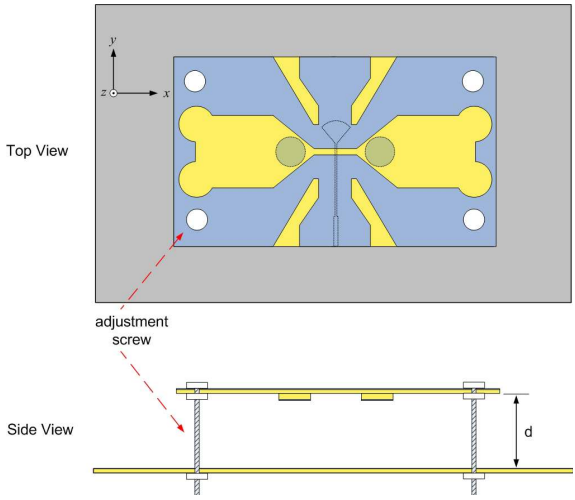

Figure 11. The configuration of the antenna with distance adjustable back reflector.

3. DESIGN OF THE ANTENNA WITH BACK-REFLECTOR

In order to obtain the desired unidirectional radiation pattern, a metallic reflector is placed behind the antenna as shown in Figure 11. According to the image principle, when the reflector is placed approximately $\lambda/4$ behind the radiator, the in-phase wave from the reflector enhances the unidirectional radiation. Inspired by that case, 4 length-adjustable screws are implemented to fix the array and the back reflector. The distance between the radiator and the reflector (d) can be easily adjusted, expecting to obtain the stable high gain in a wide frequency range.

The prototype of the reflector-backed antenna is also fabricated and shown in Figure 12. A metallic reflector with dimensions 170 mm $\times$ 240 mm is placed behind the antenna. Since the distance between the radiator and the reflector is tunable, the return loss performances of the antenna with five different d values are measured and shown in Figure 13. Thanks to the relatively long distance between the radiator and the reflector, when $d = 72.5$ mm, the impedance bandwidth covers from 0.84 GHz to 2.78 GHz (107%) with 10 dB return loss, close to the simulated antenna relative bandwidth in Section 2 (106%), excepting a slight frequency offset to lower frequencies, which is possibly due to the overall physical size increase. As Figure 13 depicted, when d decreases, the high-end cut-off the operating band shifts to higher frequencies and the low-end cut-off is restricted simultaneously, resulting in operating bandwidth shrinks. In fact, as the distance between the antenna and the reflector decreases, the lower band no longer useful; so only the higher band should be taken into consideration. When $d = 26.5$ mm, the high-end cut-off increases to 3.04 GHz. According to the return loss performances and image principle, five working status are defined

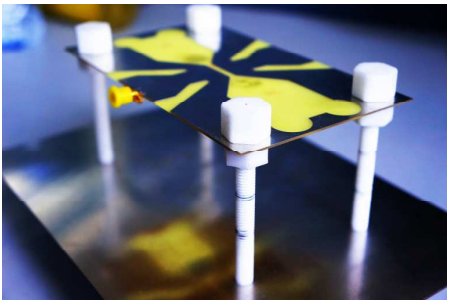

Figure 12. The photography of the fabricated antenna.

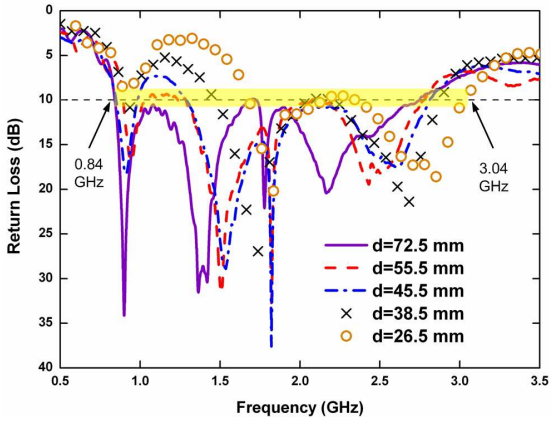

Figure 13. Measured return loss performances with different d values.

Table 2. Useable band list.

Name	Distance between the antenna and the reflector (d)	Corresponding usable frequency band coverage
Status 1	72.5 mm	0.84 GHz–1.15 GHz
Status 2	55.5 mm	1.15 GHz–1.40 GHz
Status 3	45.5 mm	1.40 GHz–1.90 GHz
Status 4	38.5 mm	1.90 GHz–2.50 GHz
Status 5	26.5 mm	2.50 GHz–3.04 GHz

and named Status 1 to Status 5, making the total available operating band covers from 0.84 GHz to 3.04 GHz (113.4%). The corresponding usable frequency ranges are listed in Table 2.

The simulated and measured normalized radiation patterns of the antenna at different statues are illustrated in Figure 14. The radiation patterns are normalized and shown in both yoz-plane and xoz-plane. As the figure indicates, the simulated and measured results agree well. Compare with the results in Figure 10, the backward ($-z$-direction) radiations are suppressed by the metallic reflector. Desired unidirectional patterns are obtained in the entire band. The Cross Polarization levels in the maximum radiation directions are less than -25 dB in all the measured frequencies. The HPBWs (half power beam widths) of the antenna are also measured and shown in Figure 15.

In the figure, the *yoz*-plane HPWB is generally varies between 45° and 70°, which is more stable compared with the one of *xoz*-plane as frequency varies. It also can be seen when the distance between the antenna and the reflector is short enough (Status 5), very wide HPBW up to 120° is obtained in *xoz*-plane since the grating lobes in Figure 10(e) merge with each other.

The front to back (F/B) ratio and antenna realized gain is also calculated based on tested results. As in Figure 16(a), the F/B ratio increases as the radiator-reflector distance gets shorter. From the figure, the greater than 8 dB F/B ratio is obtained from 0.85 GHz to 1 GHz and the greater than 14 dB F/B ratio is obtained from 1.0 GHz to more than 3 GHz. Figure 16(b) shows the gain performances of the antenna with different radiator-reflector distances in their better than

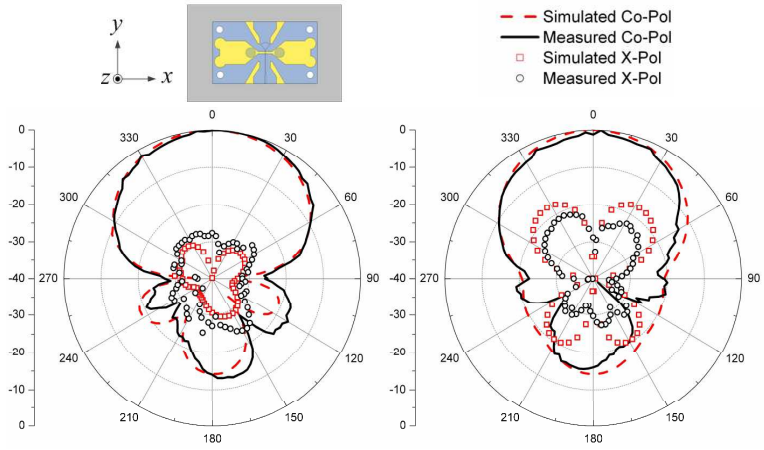

(a)

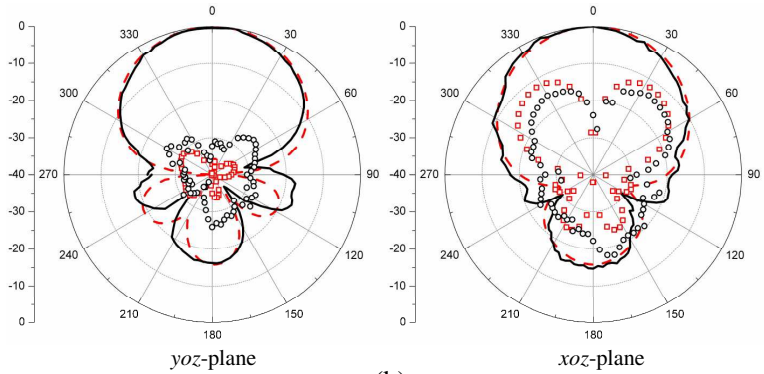

(b)

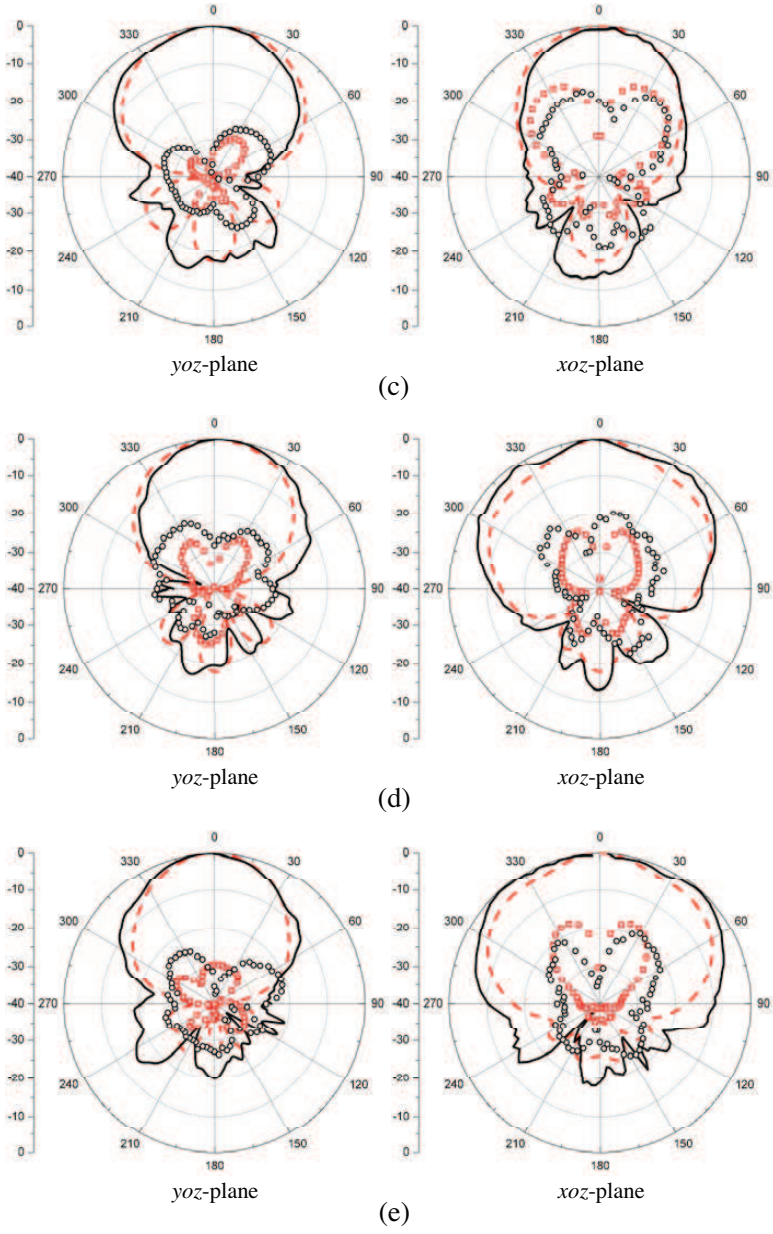

Figure 14. The normalized radiation patterns (in dB) of the reflector-backed antenna. (a) Status 1, 1.0 GHz; (b) Status 2, 1.35 GHz; (c) Status 3, 1.65 GHz; (d) Status 4, 2.25 GHz and (e) Status 5, 2.85 GHz.

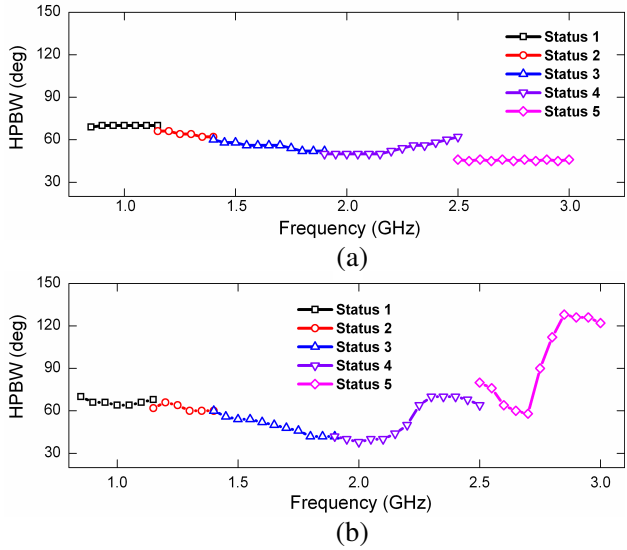

Figure 15. The (a) *yoz*-plane and (b) *xoz*-plane HPBW.

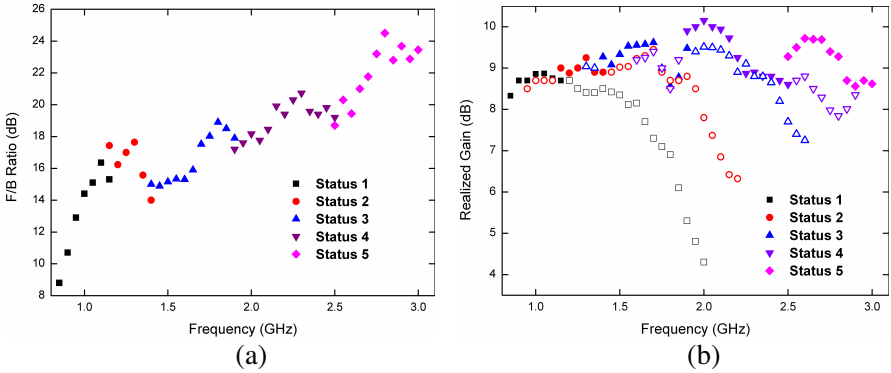

Figure 16. (a) The F/B ratio and (b) realized gain of the antenna.

10 dB return loss bands (as shown in Figure 13). In this figure, the solid dots depict the gain in the usable bands (as shown in Table 2) and the hollow dots depict the realized gains out of the usable bands. As the figure illustrated, the realized gains reach peak values in their usable bands, suggesting that the five statuses defined in Table 2 behave the best in their corresponding bands. The curves also indicate that the stable high gain is realized in the working band. Generally, the realized gain varies between 8.3 dB and 10.1 dB in the working band. The drop

of the gain in middle frequencies is primarily caused by the resonance in around 1.8 GHz.

4. CONCLUSION

In this paper, a reconfigurable WSLA installation is presented. Pony ear shaped slots and uplifted disc patch loadings are employed to enhance the impedance bandwidth. A back-reflector is introduced with adjustable distance to the radiator. Five working statuses with different radiator-reflector distances are defined for different working frequencies. The total available operating frequency ranges from 0.84 GHz to 3.04 GHz with better than 10 dB return loss. The radiation properties of the array are tested in an anechoic chamber. Stable unidirectional radiation patterns to $+z$-direction are observed in the working band with high F/B ratios. Measured results also show that the better than 8.3 dB gains are available in the entire working band. The appreciated wide frequency band coverage and stable radiation performance make the antenna a feasible substitute for multiple narrowband antennas. More importantly, the simple straightforward arrangement is cost-effective for mass production, since it eases antenna designs and manufactures, solves storage and inventory problems. This design concept in the paper offers a promising solution in industrial fields due to the mentioned advantages.

REFERENCES

1. Meena, R. and A. R. Harish, "Parasitically loaded wideband CPW-fed tapered slot antenna," *Journal of Electromagnetic Waves and Applications*, Vol. 25, Nos. 17–18, 2399–2408, 2011.
2. Li, Y.-S., X.-D. Yang, C.-Y. Liu, and T. Jiang, "Analysis and investigation of a cantor set fractal UWB antenna with a notch-band characteristic," *Progress In Electromagnetics Research B*, Vol. 33, 99–114, 2011.
3. Mao, J. Y., Z. R. Li, Q. X. Guo, H. Zhang, X. Q. Zhang, X. F. Wu, and Y. Yang, "A wideband Quasi-Yagi antenna with arrow-shaped dipoles for digital TV band applications," *Journal of Electromagnetic Waves and Applications*, Vol. 26, No. 13, 1716–1723, 2012.
4. Lin, S., Y. Tian, J. Lu, D. Wu, J.-H. Liu, and H.-J. Zhang, "A UWB printed dipole antenna and its radiation characteristic analysis," *Progress In Electromagnetics Research C*, Vol. 31, 83–96, 2012.

5. Islam, M. T., R. Azim, and A. T. Mobashsher, "Triple band-notched planar UWB antenna using parasitic strips," *Progress In Electromagnetics Research*, Vol. 129, 161–179, 2012.
6. Yang, Y., Y.-Z. Yin, Y.-Q. Wei, B.-W. Liu, and A.-F. Sun, "A circular wide-slot antenna with dual band-notched characteristics for UWB applications," *Progress In Electromagnetics Research Letters*, Vol. 23, 137–145, 2011.
7. Ren, F. C., F. S. Zhang, B. Chen, G. Zhao, and F. Zhang, "Compact UWB antenna with dual band-notched characteristics," *Progress In Electromagnetics Research Letters*, Vol. 23, 181–189, 2011.
8. Tilanthe, P., P. C. Sharma, and T. K. Bandopadhyay, "A compact UWB antenna with dual band rejection," *Progress In Electromagnetics Research B*, Vol. 35, 389–405, 2011.
9. Quan, X. L., R.-L. Li, J. Y. Wang, and Y. H. Cui, "Development of a broadband horizontally polarized omnidirectional planar antenna and its array for base stations," *Progress In Electromagnetics Research*, Vol. 128, 441–456, 2012.
10. Levy, M., S. Bose, A. V. Dinh, and D. Sriram Kumar, "A novelistic fractal antenna for ultra wideband (UWB) applications," *Progress In Electromagnetics Research B*, Vol. 45, 369–393, 2012.
11. Ta, S. X., H. Choo, and I. Park, "Wideband double-dipole yagi-uda antenna fed by a microstrip-slot coplanar stripline transition," *Progress In Electromagnetics Research B*, Vol. 44, 71–87, 2012.
12. Malekpoor, H. and S. Jam, "Ultra-wideband shorted patch antennas fed by folded-patch with multi resonances," *Progress In Electromagnetics Research B*, Vol. 44, 309–326, 2012.
13. Sagnard, F., "A compact coplanar broadband rectangular slot antenna with E-shaped feeding structure for GPR applications," *Progress In Electromagnetics Research B*, Vol. 40, 241–260, 2012.
14. Mitra, D., D. Das, and S. R. Bhadra Chaudhuri, "Bandwidth enhancement of microstrip line and CPW-FED asymmetrical slot antennas," *Progress In Electromagnetics Research Letters*, Vol. 32, 69–79, 2012.
15. Chen, Y.-C., S.-Y. Chen, and P. Hsu, "A modified CPW-fed slot loop antenna with reduced cross polarization and size," *IEEE Antennas Wireless Propog. Lett.*, Vol. 10, 1124–1126, 2011.
16. Shynu, S. V. and M. J. Ammann, "A printed CPW-fed slot-loop antenna with narrowband omnidirectional features," *IET Microw. Antennas Propag.*, Vol. 3, No. 4, 673–680, Jun. 2009.
17. Chi, P.-L., K. M. Leong, R. Waterhouse, and T. Itoh, "A

miniaturized CPW-fed capacitor-loaded slot-loop antenna," *Proc. IEEE Int. Symp. Signals, Syst. Electron.*, 595–598, Jul. 30–Aug. 2, 2007.

18. Chi, K.-C., S.-Y. Chen, and P. Hsu, "Miniaturization of slot loop antenna using split-ring resonators," *Proc. IEEE AP-S Int. Symp.*, Jun. 2009,
19. Cai, M. and M. Ito, "New type of printed polygonal loop antenna," *Proc. Inst. Elect. Eng.*, Vol. 138, Pt. H, No. 5, 389–396, Oct. 1991.
20. Mandal, M. K. and Z. N. Chen, "Compact dual-band and ultrawide band loop antennas," *IEEE Trans. Antennas Propagat.*, Vol. 59, No. 8, 2774–2779, 2011.
21. Low, X. N., Z. N. Chen, and T. S. P. See, "A UWB dipole antenna with enhanced impedance and gain performance," *IEEE Trans. Antennas Propagat.*, Vol. 57, No. 10, 2959–2966, 2009.
22. Lin, X.-C. and L.-T. Wang, "A broadband CPW-fed loop slot antenna with harmonic control," *IEEE Antennas Wireless Propog. Lett.*, Vol. 2, No. 1, 323–325, 2003.
23. Schantzand, H. and M. Barnes, "The COTAB UWB magnetic slot antenna," *IEEE Intern. Symp. on AP*, Vol. 4, 104–107, Jul. 2001.
24. Leib, M., M. Frei, and W. Menzel, "A microstrip-fed ultra-wideband slot antenna," *Proc. IEEE AP-S Int. Symp.*, Jun. 2009.
25. Wang, N. B., Y. C. Jiao, L. Zhang, Y. Song, and F. S. Zhang, "A simple low-loss broadband 1–14 GHz microstrip-to-slotline transition," *Microwave and Optical Technology Letters*, Vol. 51, 2236–2239, 2009.
26. Fei, P., Y. C. Jiao, W. Hu, and F. S. Zhang, "Microstrip to slotline transition with a 22 : 1 bandwidth," *Journal of Electromagnetic Waves and Applications*, Vol. 26, Nos. 11–12, 1500–1506, 2012.